Magnetic Nanoclusters Exhibiting Protein-Activated Near-Infrared Fluorescence

Michael A. Daniele, Margaret L. Shaughnessy, Ryan Roeder, Anthony Childress, Yuriy P. Bandera, and Stephen Foulger*

Center for Optical Materials Science and Engineering Technologies, Department of Materials Science & Engineering, Clemson University, Clemson, South Carolina 29634-0971, United States

ABSTRACT Composite nanoclusters with chemical, magnetic, and biofunctionality offer broad opportunities for targeted cellular imaging. A key challenge is to load a high degree of targeting, imaging, and therapeutic functionality onto stable metal-oxide nanoparticles. Here we report a route for producing magnetic nanoclusters (MNCs) with alkyne surface functionality that can be utilized as multimodal imaging probes. We form MNCs composed of magnetic Fe_3O_4 nanoparticles and poly(acrylic acid-*co*-propargyl acrylate) by the co-precipitation of iron salts in the presence of copolymer stabilizers. The MNCs were surface-modified with near-infrared (NIR) emitting fluorophore used in photodynamic therapy, an azide-modified indocyanine green. The fluorophores engaged and complexed with bovine serum albumin, forming an extended coverage of serum proteins on the MNCs. These proteins isolated indocyanine green fluorophores from the aqueous environment and induced an effective "turn-on" of NIR emission.

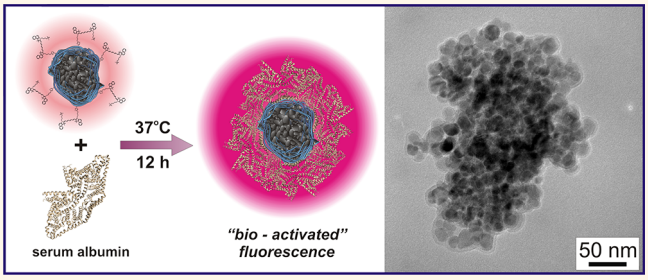

KEYWORDS: biomedical imaging · magnetic colloid · click chemistry · biodetection

Magnetic metal-oxide nanoparticles (MMOx-NP) with designer surface chemistries are candidates for the next-generation of cancer theranostics,[1,2] including diagnostic assays,[3] MRI contrast agents,[4] cell differentiation,[5] immunostimulation,[6] hyperthermia,[7] and drug delivery.[8] However, agglomeration of nanoparticles with a large surface-to-volume ratio will result in the loss of magnetic characteristics, decrease of surface activity, rapid detection, and elimination from *in vivo* circulation. In light of the aforementioned benefits and hurdles, a major challenge in nanomedicine is to devise a methodology to maintain superparamagnetism with highly stable MMOx-NP/polymer conjugates. An ideal theranostic MMOx-NP will (1) avoid ferrimagnetic agglomeration, (2) be sterically stable to prevent agglomeration in physiological media, and (3) provide surface functionality for easy chemical modification.

To attain superparamagnetic magnetite, nanoparticles smaller than ~20 nm are commonly synthesized by co-precipitation of ferric and ferrous salts.[9] Although these discrete particles are superparamagnetic, the force acting on a nanoparticle in a magnetic field is proportional to the particle size; thus, discrete nanoparticles require the application of large magnetic fields for *in vivo* activity. Large-volume MMOx-NPs are ferrimagnetic and require excess stabilizers to overcome agglomeration, so magnetic nanoclusters (MNCs) of discrete nanoparticles are most desirable because the spins on neighboring particles do not influence the total magnetization, and large volume provides for high activity in smaller magnetic fields.[10−12] MNCs are composites of adjacent iron oxide nanoparticles, aggregated with polymer stabilizers. The size and shape of polymer-stabilized nanoclusters have been controlled with block copolymers[11,13] and proteins;[14] however, the degree of functionality has been limited because of the need for a large amount of stabilizing agents. To attain novel surface chemistries, discrete nanoparticles and MNCs are usually modified from an oleic acid coating or treated with sophisticated

* Address correspondence to foulger@clemson.edu.

Received for review August 16, 2012 and accepted December 3, 2012.

Published online December 03, 2012
10.1021/nn3037368

ligand exchange reactions to modify the surface moiety for subsequent attachment of desired molecules.[15−17] Ligand exchange reactions commonly require nonaqueous solvents, harsh conditions, and multistep protection sequences that are not amenable to high-efficiency functionalization or high-throughput production.

Unlike the direct surface functionalization of MMOx-NPs, the polymer stabilizers required for MNC synthesis have the potential to incorporate a myriad of surface functional groups in a single step by designing and employing novel copolymer stabilizers. An ideal magnetic nanocluster functionality, which has been difficult to achieve, is the preparation of MMOx-NPs for ready use in the copper(I)-catalyzed azide alkyne cycloaddition (CuAAC) reaction. CuAAC reactions are a typical example of the "click reaction" (aqueous compatibility, high yield, oxygen insensitive, and orthogonal chemistry)[18] and have been widely applied in the fields of drug development and biomacromolecule modifications.[19] Few efforts have been made to modify magnetic nanoparticles for click chemistry without direct ligand exchange on the surface of the particles. Prior efforts have demonstrated routes for coating individual nanoparticles with poly(acrylic acid) and proceeding with EDC coupling reactions to exchange carboxylates for alkyne functionality.[20] However, these efforts required multiple labor-intensive synthesis steps to provide an alkyne functionality. To meet the demand for the rapid development of commercially applicable magnetic nanoparticles, high-throughput surface coating and functionalization procedures must be synchronized.

Herein, we report the synthesis and characterization of "clickable" magnetic nanoclusters and their development as bioimaging tools which exhibit protein-activated NIR fluorescence. Prior efforts have exploited the formation of MNCs to increase bioimaging sensitivity,[21,22] but to date, there has been no effort to incorporate a functional moiety onto the surface of the MNCs. Therefore, the design of our polymer stabilizers incorporated a chemisorbed stabilizer (acrylic acid) with an alkyne-bearing comonomer (propargyl acrylate). Addition of the alkyne functional group provided for the use of the CuAAC reaction, which is a facile and versatile chemistry for bioconjugation. Unlike previously reported MNCs, our magnetic nanoclusters (MNCs) offer (1) the ability to attain bulk magnetization response by clustering discrete nanoparticles and (2) the ability to selectively functionalize the MNCs with a click transformation. The MNCs composed of discrete iron oxide (Fe_3O_4) nanoparticles and copolymer stabilizers exhibited near bulk magnetization response (~93 emu · g^{-1}), which is greater than that of discrete superparamagnetic nanoparticles. More importantly, the addition of the alkyne functional group was exploited *via* the conjugation of an azide-modified, theranostic fluorophore on the surface of the MNCs. The attachment of azICG-induced serum albumin binding formed a fluorescence-enhancing microenvironment around the attached fluorophores and resulted in the effective "turn-on" of NIR emission. The conjugation of MNCs and azICG provides for the constructive utilization of the surface-bound proteins and lipids that would be encountered during *in vivo* application. This system presents the blueprint for the next-generation of multimodal imaging platforms, incorporating both high sensitivity to magnetic fields and the added contrast of a "bioswitched" fluorescence.

RESULTS AND DISCUSSION

Recently, we proposed a method for the click functionalization of nanoparticles by polymerization of a *clickable* shell onto a polystyrene core.[23] To this end, we utilize a functional copolymer to form iron oxide nanoparticles into MNCs. Figure 1a1 presents a schematic of the procedure employed to synthesize fluorescent MNCs. The iron oxide nanoparticles were prepared using a modified chemical co-precipitation of iron salts with a strong base. To aggregate the iron oxide nanoparticles and form stable MNCs, the synthesized copolymers were incorporated as aqueous solutions with the iron salts. To achieve alkyne functionality, poly(acrylic acid-*co*-propargyl acrylate) was used as the stabilizer. The carboxylate groups of poly(acrylic acid) bind to the MMOx-NP surface, and propargyl acrylate acts as the functional comonomer due to its general application in click reactions, including CuAAC and thiol-yne additions.[18,24] Subsequently, the surfaces of the MNCs were modified *via* the CuAAC reaction between the alkyne-functionalized stabilizer and a Food and Drug Administration approved near-infrared (NIR) emitting fluorophore and theranostic moiety, indocyanine green (ICG, λ_{ex} = 780 nm, λ_{em} = 820 nm).[25,26] The ICG moiety was modified with an azide functionality (azICG). Due to the mild reaction conditions, high conversion rate, and chemoselectivity, click reactions are a powerful strategy for magnetic, fluorescent nanocomposite preparation. The CuAAC click reaction offers a good alternative to other more conventional MMOx-NP functionalization schemes that often rely on the reactivity of amine and thiol groups.[1,27] The azICG-modified MNCs were characterized using absorption and fluorescence measurements. Figure 1a2 presents the absorption and fluorescence (λ_{ex} = 725 nm) spectra of the azICG-MNCs suspended in phosphate buffered saline solution (PBS, pH = 7.4, 0.1 M). The inset of Figure 1a2 presents the uncorrected absorbance spectrum of bare-MNCs and azICG-MNCs. Bare-MNCs have a broad absorbance in the NIR wavelengths, but distinct absorbance peaks arise when ICG is functionlized to the surface. The azICG-MNCs have an absorption maximum at λ_{ex} = 800 nm and fluorescence maximum at λ_{ex} = 827 nm, with a resulting Stokes shift for the nanocluster-attached dyes of 27 nm. The fluorescent azICG-MNCs exhibit a bathochromic shift from the absorbance and emission

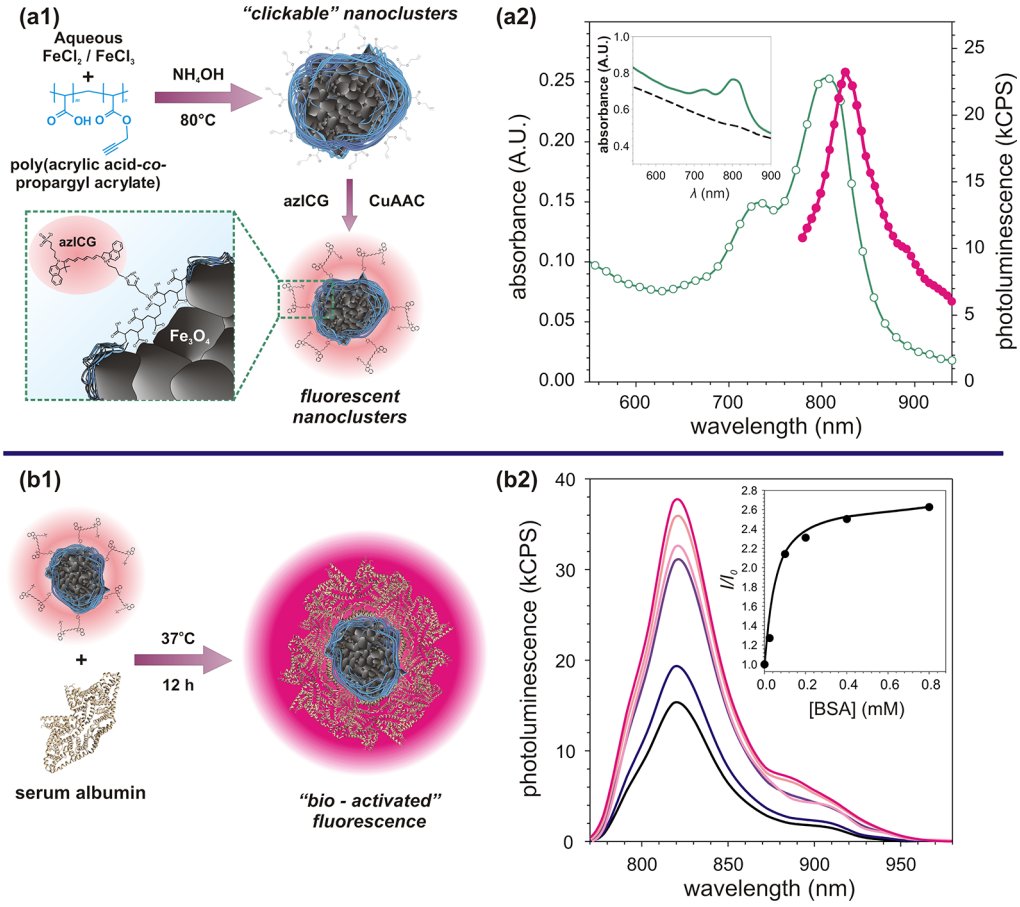

Figure 1. (a1) Schematic of the production of polymer-stabilized nanoclusters by chemisorption of poly(acrylic acid-*co*-propargyl acrylate) to Fe_3O_4 nanoparticles and functionalized with an azide-modified indocyanine green derivative (azICG) attached by CuAAC. (a2) Attachment of azICG provides absorption (○) and photoluminescence (●) response in the NIR wavelengths (λ_{ex} = 725 nm). (b2,Inset) Bare nanoclusters show a broad absorbance across the NIR wavelengths (- - -), and after modification with ICG, distinct absorption bands arise at 725 and 800 nm (—). (b1,b2) Subsequent fluorescence activation is exhibited after incubation and complexation with bovine serum albumin, (b2,inset) resulting in >250% increase in total fluorescence. Absorbance and fluorescence were measured at an MNC concentration of 1 mg·mL^{-1} in PBS.

of solvated ICG, which is expected from surface-conjugated azICG.[28] The CuAAC reaction successfully coupled azICG to the stabilizing polymer, yielding novel fluorescent MNCs.

Figure 1b1 illustrates the subsequent fluorescence *protein activation* by binding of bovine serum albumin to the surface-attached azICG. Prior efforts have shown that an initial immunoresponse to exogenous nanoparticles results in the rapid formation of a protein and lipid "corona" at the nanoparticle surface.[29] Previously considered a hindrance to the *in vivo* use of nanoparticles, recent reports have exploited the formation of the protein corona as an active component of the theranostic system.[28,30] To this extent, the azICG-MNCs were exposed to serum albumin to elicit a bioactivated fluorescence. It has been well-established that the fluorescence of high concentrations of ICG, whether aggregated in aqueous media or on a surface, is greatly diminished.[31] However, the fluorescence quantum yield of ICG can be promoted by the adsorption of the fluorescent moiety onto a macromolecule or binding with a protein.[28,32] Accordingly, the azICG-MNCs were mixed with bovine serum albumin (BSA) at increasing concentrations, and the fluorescent response was monitored after a 12 h incubation period. The observed fluorescence intensity increased with additional BSA, with the rate of increase slowing at concentrations of BSA greater than 0.25 mM (cf. Figure 1b2). The inset of Figure 1b2 presents the intensity ratio (I/I_0) for the azICG-MNCs at different BSA concentrations. The azICG-MNCs exhibit a long-term increase in total fluorescence of ~250%, where the ultimate fluorescence intensity was monitored after 60 h. The observed fluorescence activation with BSA is attributed to the ability of the protein to form a hydrophobic microenvironment at the surface of the MNCs and isolate the azICG moiety from the bulk, aqueous environment. By altering the local microenvironment of the azICG, there is an increase in quantum yield and subsequent promotion of fluorescence intensity.[28,33] The bound protein acts to "turn-on" the NIR fluorescence, while providing an effective, biomimetic surface for the MNCs, and this effect greatly increases the potential of utilizing the azICG-MNCs for directed *in vivo* imaging. Protein-activated fluorescence

has been a long-standing goal to enhance signal-to-noise ratio *in vivo*.[34,35] Multimodal fluorescence imaging is often limited by wash-out from background fluorescence. This deliterious effect has been successfully countered by the protein activation of MNC fluorescence, which enhances the contrast for imaging real-time biological events. The extent of fluorescence activation of these MNCs is dependent on the availability of azICG at the surface of the MNCs which provides binding sites for proteins, and these MNCs are a model for the array of biofunctional ligands that can be attached to the MNCs formed with functional copolymer stabilizers.

Synthesis and Characterization of Polymers. While designing functional copolymer stabilizers to carry the binding ligands and to form the iron oxide MNCs, we considered their adsorption properties and the challenges associated with incorporating bifunctional monomers. We reasoned that the intelligent incorporation of *clickable* moieties into "metal-complex" coatings will shortcut the multistep ligand exchange reactions, while providing a biocompatible, stabilizing surface. It has been established that carboxylate groups strongly complex with metal atoms in metal oxides through bidentate resonance bonding.[36−38] For our studies, we designed copolymers with a foundation of carboxylic acid groups, in the form of poly(acrylic acid), to serve as anchors which will complex with the iron atoms at the surface of the iron oxide nanoparticles.

Poly(acrylic acid) (P(AA)) and poly(acrylic acid-*co*-propargyl acrylate) (P(AA-PA)) polymers were synthesized and used to form stable MNCs. To incorporate the desired functionality, we exploited the simple free-radical copolymerization of acrylic acid with propargyl acrylate (PA), an acrylic monomer containing alkyne functionality. Propargyl acrylate is able to act as a bifunctional monomer in free-radical polymerization. The use of a chain transfer agent (CTA) for synthesis of high molecular weight, PA-containing polymer is essential because the use of even small amounts of PA can result in cross-linked gels.[39] During synthesis of the copolymer stabilizers, cross-linking was avoided by balancing the amount of the bifunctional PA monomer, polymerization time, and concentration of a CTA, 1-nonanethiol.[23] The addition of CTA also benefited the tailoring of the molecular weight and polydispersity (PDI) of the synthesized polymers.

The synthesized polymers were analyzed by FTIR spectroscopy to verify the constituency of the polymer stabilizer and presence of the incorporated alkyne functionality. FTIR spectra for the synthesized polymers used in this study (citric acid and the variants of PAA and AA-PA) are provided in the Supporting Information (Figure S1). The characteristic stretching frequencies of P(AA) include O−H stretching at 3431 cm^{-1}, C═O stretching at 1728 cm^{-1}, and the C−O stretching at 1100−1200 cm^{-1}. All spectra exhibited the series of broad peaks between 2500 and 3500 cm^{-1} attributed to the O−H stretching and bound water. The defined, strong peak at 1750 cm^{-1} is directly attributed to the C−O stretching in the carboxylates of each polymer. The FTIR spectrum of the $P(AA\text{-}PA)_{3\%,CTA}$ stabilizer clearly exhibited a peak at 2130 cm^{-1}, attributed to the alkyne functionality, while any signal at 2130 cm^{-1} for P(AA-PA) without CTA ($P(AA\text{-}PA)_{3\%}$) was within the noise level and difficult to discern.

TABLE 1. Molecular Weight Characteristics of Synthesized Poly(acrylic acid) (P(AA)) and Poly(acrylic acid-*co*-propargyl acrylate) (P(AA-PA))[a]

	M_w/M_n	PDI
P(AA)	16.6k/12.6k	1.32
$P(AA)_{CTA}$	12.8k/4.3k	2.97
$P(AA\text{-}PA)_{1\%}$	22.7k/13.9k	1.64
$P(AA\text{-}PA)_{1\%,CTA}$	17.1k/4.5k	3.79
$P(AA\text{-}PA)_{3\%}$	29.1k/13.0k	2.23
$P(AA\text{-}PA)_{3\%,CTA}$	14.3k/3.2k	4.48

[a] Subscript denotes molar percent propargyl acrylate and chain transfer agent (1-nonanethiol) used in polymerization. Molecular weights were determined by gel permeation chromatography.

Gel permeation chromatography (GPC) was performed with the synthesized polymers, and the calculated molecular weights are presented in Table 1. Polymers that did not employ CTA (P(AA), $P(AA\text{-}PA)_{1\%}$, and $P(AA\text{-}PA)_{3\%}$) exhibited number averaged molecular weights that range from 16 000 to 29 000 and have a PDI between 1.32 and 2.23. In contrast, the polymers which employed the CTA exhibited significantly lower molecular weights of 12 800−17 100 and a broader PDI between 2.97 and 4.48. The reduction of molecular weight and increase of PDI are the expected outcomes of the incorporation of the CTA.[40] The molecular weight of the stabilizers was tailored to a range that has been reported to form nanoclusters with a high polymer loading and by bridging between nanoparticles.[13] A high percent of polymer incorporation and uniform coating is critical for maintaining colloidal stability of the MNCs and to achieve an accessible alkyne functionality.

Preparation of Magnetic Nanoclusters. To prepare the MNCs, iron oxide nanoparticles were synthesized by a standard co-precipitation technique in the presence of the stabilizing polymers. As a reference, MNCs were also prepared with citric acid, which acts as a small-molecule stabilizer by an analogous carboxylate complexation with the iron oxide nanoparticles.[41−43] The copolymer-stabilized MNCs were analyzed with FTIR spectroscopy and thermogravimetric analysis (TGA) to determine their constituency. Figure 2a presents the FTIR spectra of the prepared MNCs. The peaks between 400 and 600 cm^{-1} are associated with the stretching and torsional vibration modes of the Fe_3O_4; these assignments are concordant with the two broad bands at 580 and 400 cm^{-1} associated with magnetite.[44]

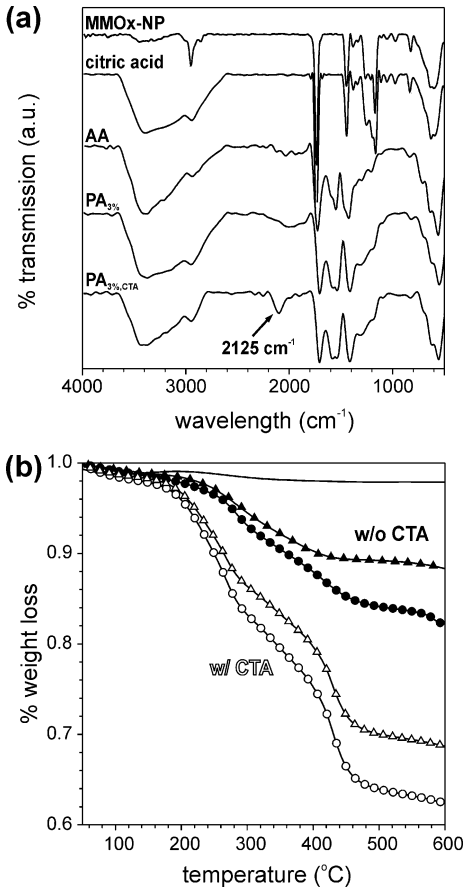

Figure 2. (a) FTIR spectra of bare iron oxide nanoparticles and polymer-stabilized nanoclusters. (b) Thermogravimetric analysis of bare iron oxide nanoparticles (—), poly(acrylic acid-*co*-propargyl acrylate) (▲, △), and poly(acrylic acid) (●, ○) stabilized nanoclusters.

All MNCs exhibit peaks at 2900 cm^{-1} (the stretching vibration of C−H groups) and 1442−1400 cm^{-1} (the bending vibration of C−H groups and asymmetric stretching of C−O groups). The broad, intense band at 3500 cm^{-1} exhibited by the citric acid and polymer-stabilized nanoclusters is attributed to structural −OH groups and incorporated water. The 1700 cm^{-1} peak is attributed to the C═O vibration (symmetric stretching) of the COOH group present in the stabilizers, which shifts to a broader band at 1600 cm^{-1}, revealing the binding of a carboxylate to the iron oxide surface.[36,37] In both cases, the position of the carboxylate asymmetric and symmetric stretching frequency exhibits a hypsochromic shift when attached to the iron oxide particle surface compared to the unadsorbed P(AA). Nonsignificant differences between the FTIR spectra of the nanoclusters were observed, suggesting a uniform mechanism of carboxylate complexation for both citric acid, P(AA), and P(AA-PA) polymer−iron binding. The FTIR spectrum of the $P(AA\text{-}PA)_{3\%,CTA}$ stabilizer exhibited a peak at 2125 cm^{-1}, attributed to the incorporated alkyne groups. Figure 2b presents the thermograms of polymer-stabilized MNCs, and the polymer content is summarized in Table 2. The degradation

TABLE 2. Characteristics of MNCs Stabilized by Citric Acid, Poly(acrylic acid), or Poly(acrylic acid-*co*-propargyl acrylate)[a]

		polymer		f_{max}[d]		
	d_{DLS}[b] (nm)	(w/w)%	d_X[c]	(kHz)	τ_{eff} (s)	τ_B (s)
citric acid	59 ± 9		31.19	15.62	0.00001	0.00001
P(AA)	278 ± 17	18.0	331.53	0.013	0.01225	0.00738
$P(AA)_{CTA}$	225 ± 19	37.6	316.09	0.015	0.01062	0.00391
$P(AA\text{-}PA)_{3\%}$	162 ± 10	11.7	131.99	0.206	0.00077	0.00146
$P(AA\text{-}PA)_{3\%,CTA}$	136 ± 6	31.3	71.43	1.330	0.00012	0.00086

[a] Subscript denotes molar percent PA and use of chain transfer agent. Polymer (w/w)% was measured by thermogravimetric analysis. [b] Hydrodynamic diameter of nanoclusters as measured by dynamic light scattering. [c] Hydrodynamic diameter of nanocluster derived from low-frequency AC susceptometry. [d] Frequency at maximum absorbance for the imaginary component of complex susceptibility; τ_{eff} and τ_B were calculated from eqs 1 and 2, respectively.

between 200 and 400 °C is attributed to the thermal degradation of P(AA), the primary polymer constituent of the MNCs. The polymer content ranged between 11 and 38% (w/w), with the highest polymer content in systems that utilized CTA. Both the lower molecular weight and higher PDI of polymers synthesized with CTA contributed to the increased polymer content of the nanoclusters. For polymers with higher PDI, the array of molecular weights acts as a mosaic coating in which secondary polymer chains can "pack" onto the nanocluster.[13] The range of polymer content realized by tailoring the molecular weight and PDI is a benefit for optimizing MNC formation.

The control of the polymer loading also effects the stability of MNCs in an array of aqueous environments. The stability of the MNC is dependent on electrosteric repulsion over a range of pH values, which would be encountered for both *in vitro* and *in vivo* applications. MMOx-NPs, while capable of being suspended in water, aggregate due to attractive van der Waals forces; thus, we investigated the stabilizing effects of the copolymer for MNCs suspended in a range of aqueous buffers. The reported MNCs would be sterically stabilized by the polymer coating of the iron oxide surface; moreover, the formed MNCs are electrostatically stabilized due to the choice of a polyelectrolyte as the MNC-forming polymer. The stability of the MNCs was assessed by ζ-potential analysis. The MNCs were considered stable, due to the mutual electrosteric repulsion, when the absolute ζ-potential is greater than 30 mV.[45] In the case of the nanoclusters, the acid groups of all stabilizers would provide a negative surface charge and MNC repulsion. Figure 3 presents the ζ-potential of the citric acid, P(AA), and P(AA-PA) formed nanoclusters. Salt concentration was maintained at a relatively high level, 0.1 M, to ensure a high ionic strength at the extremes of the pH range. Excellent stability is exhibited for all nanoclusters at $5 < pH < 9$, with the ζ-potential values in this range of pH falling below −30 mV. An isoelectric point is clearly realized for citric acid formed MNCs (Figure 3a) at pH <2.

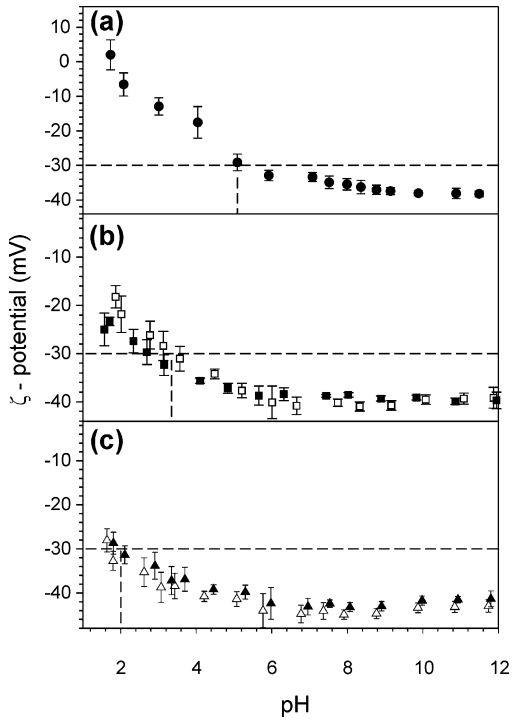

Figure 3. Zeta-potential of (a) citric acid, (b) P(AA), and (c) P(AA-PA)$_{3\%}$ formed magnetic nanoclusters, polymerized with (filled) and without (open) chain transfer agent. Dotted lines signify stable ζ-potential, where ζ ≤ −30 mV.

The higher loading of polymers in the MNC provides better stability, as illustrated by the shift where the ζ-potential exceeds −30 mV. At pH <6, there is a sharp increase in the ζ-potential for the citric acid MNCs. The destabilization is caused when the carboxylate group in the citric acid nanoclusters is protonated at pH ≤5.5.[36] The polymer-stabilized MNCs demonstrate a similar effect at pH <5.5; however, the abundance of polymer maintains ζ-potential values less than −30 mV until a pH <3 is reached. Being highly stable in this broad range of aqueous buffers, the polymer-stabilized MNCs are suitable for any number of surface-conjugation reactions and physiological applications.

Characterization of Iron Oxide Nanoparticle Formation and Clustering. MNC formation can be initiated by two mechanisms: (1) reduction of surface energy of the nanoparticles followed by the chemisorption of polymer to the nanocluster surface or (2) bridging of an extended network of hydrated polymers between individually coated nanoparticles. The predominant formation route is dictated by the molecular weight of the stabilizer, where a minimum in nanocluster size is exhibited by individually coated nanoparticles, followed by a sharp rise in nanocluster diameter as molecular weight increases and bridging occurs.[13] To better understand the effect of molecular weight and PDI on the *in situ* formation of MMOx-NPs into MNCs, the arrays of prepared MNCs were characterized with HR-TEM, dynamic light scattering (DLS), and AC susceptometry; the characteristics of the MNCs are summarized in Table 2.

Figure 4a presents HR-TEM micrographs of an illustrative MNC, formed with P(AA-PA)$_{3\%,CTA}$. The polymer-stabilized MNCs are composed of densely aggregated Fe_3O_4 nanoparticles, as illustrated in Figure 4a1 (the characteristic 2.54 Å lattice spacing corresponds to the *d* value of the [311] plane of Fe_3O_4).[46] At lower magnification, we can also resolve that the MNCs were composed of primary Fe_3O_4 crystals between 5 and 20 nm (well within the superparamagnetic regime) and a 5−10 nm stabilizing cap of copolymer (additional micrographs are provided in Figure S2). Vibrating scanning magnetometry was utilized to measure the magnetic properties of the synthesized MNCs, and a representative magnetization curve of the polymer-stabilized MNCs is provided in Figure S4. The MNCs exhibited ferromagnetic behavior with minimal hysteresis attributed to the resultant polydispersity of nanoparticle size due to the co-precipitation of Fe_3O_4 nanoparticles (H_c < 0.02 kOe).[47] The saturation magnetization was *ca.* 93 emu·g^{-1}, which is the theoretical magnetization value of magnetite at room temperature (90−100 emu·g^{-1}).[48] The near superparamagnetic behavior is attributed to the discrete MMOx-NPs within the MNCs, and the high saturation magnetization is attributed to the ability of the polymer stabilizers to form large clusters of the discrete MMOx-NPs. The increased size of the clusters provides for optimized coupling with the applied magnetic field.

The size of the MNCs was determined by DLS, and the mean hydrodynamic diameter and standard deviation are provided in Table 2. The MNCs ranged from 50 to 300 nm dependent on molecular weight of the agent applied for cluster formation. The citric-acid-stabilized nanoclusters had the smallest hydrodynamic diameter of 59 nm. The clustering of citric-acid-stabilized MNCs are solely attributed to the minimization of the Fe_3O_4 surface energy, as the citric acid coating does not shield against the van der Waals attractive interaction between MMOx-NPs.[49] The mean hydrodynamic diameter was 278 and 162 nm for P(AA) and P(AA-PA) nanoclusters, respectively. The average diameter for nanoclusters formed with P(AA)$_{CTA}$ and P(AA-PA)$_{CTA}$ was significantly smaller, 228 and 136 nm. MNC size has been shown to be a function of polymer molecular weight and PDI, in which MMOx-NP aggregation dominates at low molecular weight and stabilizer bridging forms MNCs at higher molecular weight.[13] Therefore, the use of CTA generates polymers with low molecular weight and high PDI, where the smaller chains may more efficiently coat the MMOx-NPs, producing smaller MNCs. As the molecular weight increases and PDI decreases, bridging between the unstable MMOx-NPs occurs and the hydrodynamic diameter of P(AA) and P(AA-PA) MNCs is shown to increase. The molecular weight and PDI of the stabilizing copolymers have a clear effect on the hydrodynamic size of these MNCs, suggesting that the

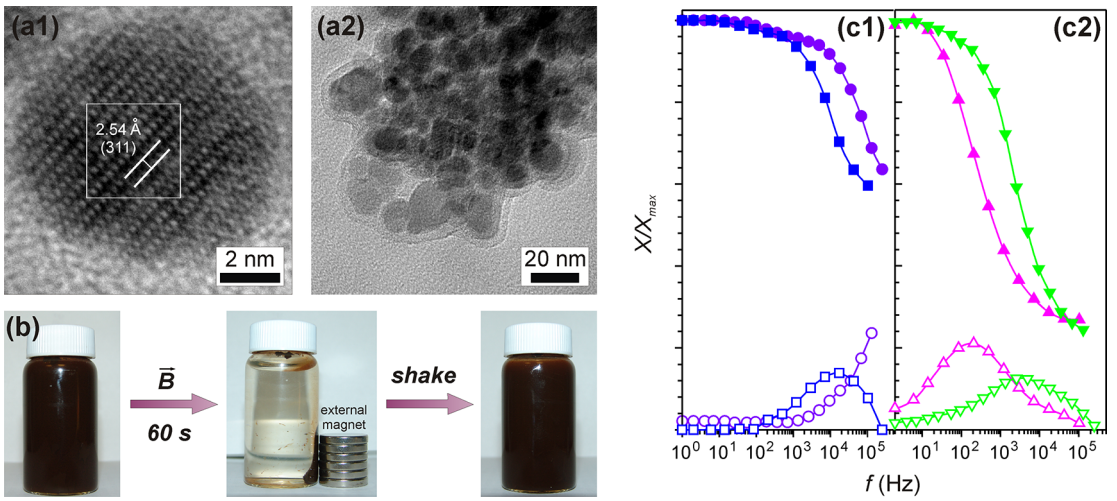

Figure 4. (a1) HR-TEM micrographs of P(AA-PA)-stabilized nanoclusters exhibiting the crystallinity of the Fe_3O_4 particles and the [311] plane with lattice spacing of 2.54 Å, and (a2) copolymer stabilizer coating on the surface of the nanocluster. (b) MNCs under an applied external magnetic field are segregated and then easily redistributed after removal of the external magnetic field. (c1,c2) AC susceptibility measurements in the range of 1−100 kHz, $X'(\omega)$ (filled) and $X''(\omega)$ (open) *versus* (c1) bare nanoparticles (○, purple), citric-acid-stabilized nanoclusters (□, blue), and (c2) P(AA-PA) (Δ, pink) and $P(AA\text{-}PA)_{CTA}$ (▽, green) nanoclusters.

stabilizer characteristics also affect the mechanism of cluster formation.

To further examine MNC formation, AC susceptometry was employed to correlate magnetic relaxation times to nanocluster size distributions and cluster constituency. The characteristic relaxation times of MMOx-NPs are highly sensitive to the surface chemistry, and this property can be exploited as a probe in magnetic biotechnologies, including protein binding assays[1,50,51] and hyperthermia therapeutics.[7] There are two distinct mechanisms by which the magnetization of the MNCs may relax after an applied magnetic field has been removed: (1) bulk rotation of the MNC within the carrier liquid (Brownian relaxation) or (2) rotation of the magnetic vector within the MMOx-NP (Néel relaxation). In a sample with a distribution of MMOx-NP and MNC size, both relaxation mechanisms will contribute to an effective relaxation, τ_{eff}. The effective relaxation time is dominated by the faster mechanism and is described in eq 1, where τ_B and τ_N are the Brownian and Néel relaxation times, respectively. When iron oxide MNCs are formed by surface-energy minimization of nanoparticles prior to polymer stabilization, the proximity of the nanoparticles causes nondiscrete magnetic response, the nanoparticles become confined, and Néel relaxation dominates.[52] However, the polymer-stabilized MNCs exhibit segregated magnetic properties, where the MNCs relax by the Brownian mechanism.[53−55]

$$\tau_{eff} = \frac{\tau_B \tau_N}{\tau_B + \tau_N} = \frac{1}{2\pi f_{max}} \quad (1)$$

Measurement of the frequency-dependent susceptibility provides a route to analyzing the clustering mechanism by measuring the dominant relaxation mechanism. The frequency-dependent susceptibility may be written in terms of its real and imaginary components, where the complex susceptibility has a frequency dependence fitted to the Debye model for dielectric dispersions.[56] This model utilizes an effective relaxation time that is dependent on the excitation frequency when the imaginary component of the complex susceptibility attains a maxima, f_{max} (cf. eq 1). By measuring the excitation frequency at which $X''(\omega)$ attains a maxima, we can calculate a "magnetic" size distribution and determine the effective relaxation time. The frequency-dependent susceptibility was measured from $1 \leq f \leq 250$ kHz, and results are summarized in Table 2.

Figure 4c presents the normalized plots of the real ($X'(\omega)$) and imaginary ($X''(\omega)$) components of the complex susceptibility for (c1) iron oxide nanoparticles *versus* citric-acid-stabilized MNCs and (c2) P(AA-PA) and $P(AA\text{-}PA)_{CTA}$-stabilized nanoclusters. In the ideal Debye case, the predicted intersection of the real and imaginary components occurs at the maxima of X'', when $\omega\tau_{eff} = 1$ and $X''(\omega)_{max} = 0.5$.[54,55] For iron oxide nanoparticles, f_{max} would be realized at $f > 1$ MHz, which results in relaxation times in the domain of the Néel mechanism because the formation of MNCs by iron oxide nanoparticles is caused by the reduction of nanoparticle surface energy. The citric-acid-stabilized MNCs also exhibit $X''(\omega)_{max}$ at higher frequency but have a clear local maxima at *ca.* 15 kHz. The citric-acid-stabilized MNCs exhibit some Brownian relaxation.

Upon the addition of cluster-forming stabilizers, the $X''(\omega)$ maxima shifts toward lower frequencies as exhibited by the P(AA-PA) MNCs synthesized with and without CTA (cf. Figure 4c2). A comparable trend is exhibited by the P(AA) MNCs (cf. Figure S3). The shift toward low-frequency absorption is indicative of the increased effect of the Brownian relaxation mechanism.

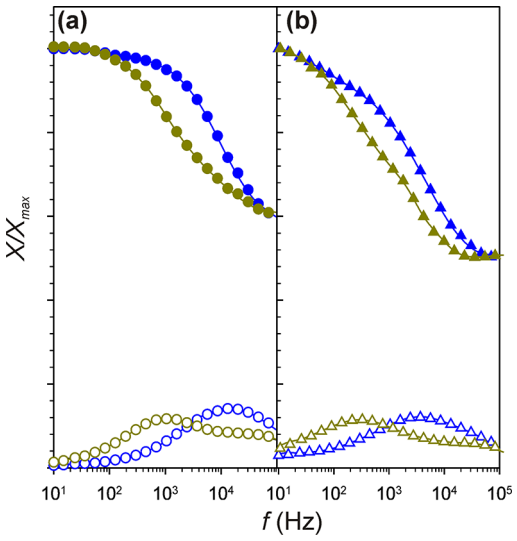

Figure 5. Plot of normalized magnetic susceptibility, $X'(\omega)$ (filled) and $X''(\omega)$ (open), agianst frequency for (a) citric acid (○) and (b) P(AA-PA) (Δ) nanoclusters in water (blue) and glycerol solution (gold).

In Figure 4c2, there is also a significant shift in the maximum absorbance frequency between P(AA-PA) synthesized with and without CTA. This shift corroborates the increased MNCs' size exhibited in DLS measurements, as the larger P(AA-PA) MNCs have a maximum absorbance at lower frequency than the $P(AA\text{-}PA)_{CTA}$. The lower frequency results in a longer relaxation time, attributed to the Brownian mechanism. The characteristic rotational diffusion times of the Brownian relaxation mechanisms are realized at lower frequencies as given by eq 2, where η is the dynamic viscosity the carrier fluid and r is the hydrodynamic radius. The hydrodynamic radii and calculated relaxation times are summarized in Table 2. The calculated τ_{eff} values, derived from low-frequency AC susceptometry, are within the Brownian time domain ($5 \times 10^{-5} - 0.02$ s) for all MNCs. The time domain of τ_{eff} is also comparable to that of τ_B as calculated from eq 2 using the DLS measured hydrodynamic radius of the MNCs. This correlation suggests that the Brownian relaxation mechanism is the dominant magnetic relaxation route for the MNCs.

$$\tau_B = \frac{4\pi\eta r^3}{kT} \qquad (2)$$

To verify the dominant effect of Brownian relaxation in the polymer-stabilized MNCs, the complex susceptibility was measured at an increased viscosity, by changing the carrier liquid from water (8.8×10^{-4} Pa·s) to glycerol (50 (v/v)%, 6.7×10^{-3} Pa·s) at 25 °C (cf. Figure 5).[53] MNCs exhibit a significant shift toward a lower f_{max} due to viscosity change, as would be expected from the Brownian relaxation mechanism. At higher viscosity, the lower f_{max} correlates to a longer τ_B. However, the relative absorbance peak is unchanged, suggesting that the stabilizing agent keeps the MMOx-NPs isolated and the MNCs relax as a whole, not as discrete particles.

The relaxation of the MNCs is ultimately a distribution of both the Brownian and Néel mechanisms. For ideal MMOx-NPs, the imaginary susceptibility attains a maximum of 0.5 (X''_{max}).[55,56] For these synthesized MNCs, $X''_{max} < 0.5$; therefore, the nanoclusters will exhibit another local maxima at higher frequency attributed to the Néel relaxation mechanism.[54,57] The distribution of the $X''(\omega)$ absorption is evidence of the distribution of relaxation mechanisms within the nanoclusters and is most apparent when comparing the imaginary components of the bare iron oxide nanoparticles, citric-acid-stabilized and P(AA-PA) MNCs (cf. Figure 4c). For the P(AA-PA) MNCs, the absorbance at low frequency is indicative of a dominant Brownian relaxation effect, whereas the bare nanoparticles and citric-acid-stabilized MNCs exhibit negligible absorbance in this range, intimating an absorbance distribution at higher frequency caused by Néel relaxation. This suggests that the MNCs are composed of (1) a core of electrostatically aggregated iron oxide nanoparticles and (2) a solvent-accessible volume of polymer-stabilized nanoparticles aggregated by the bridging of the attached stabilizer. The electrostatically aggregated nanoparticles exhibit Néel relaxation, while the solvent-accessible polymer−nanoparticle bridges at the surface of the MNCs account for the dominant Brownian relaxation mechanism, as monitored by AC susceptometry.[54] The combination of surface-energy minimization and polymer-bridge clustering explains the comparably high loading of polymers in the nanoclusters; that is, the polymers penetrate through the volume of the nanocluster. The segregation of MMOx-NPs in the MNCs by the copolymer-stabilizer preserves the magnetic properties of discrete MMOx-NPs while reducing the applied field necessary for magnetic response. Therefore, the aggregated nanoparticles can affect a much large magnetic force, while the polymer-bridged component provides for nanocluster stability, which is a beneficial consequence for applications such as magnetic hyperthermia or magnetic drug delivery where strong magnetic response is preferred but polymeric functionalization and stealth is often required.

CONCLUSIONS

In this study, we demonstrated protein-activated NIR fluorescence using copolymer-stabilized MNCs. Recent efforts have begun to explore the utility of polymer-stabilized MNCs,[11,22] and in this effort, we successfully demonstrated and characterized a general methodology for producing MNCs with an alkyne functionality for use as NIR fluorescing probes. The functional MNCs were formed by the adsorption of poly(acrylic acid-*co*-propargyl acrylate) onto iron oxide nanoparticles, which provided both colloidal stability and surface functionality. Complicated synthesis routes previously required for the surface functionalization of magnetic nanoparticles are circumvented by designing the functional copolymer

stabilizer prior to MNC formation. By copolymerizing acrylic acid with propargyl acrylate, we synthesized a *clickable* coating that would be anchored to the iron oxide surface. We also demonstrated the size of the nanoclusters, and thickness of the polymer coating was controlled by tailoring the molecular weight of the adsorbed polymer with the use of a chain transfer agent during synthesis. The complex susceptibility measurements of the particles were utilized to investigate the nanoparticles clustering formation. Nanoclusters exhibited a relaxation time dominated by Brownian relaxation, confirming that the particles coat with polymer and then bridge to form clusters. The availability of alkyne groups on the surface of the aqueous-phase nanoclusters allowed for the surface modification of the MNCs *via* the CuAAC reaction. A theranostic moiety, azICG, was utilized for both its NIR fluorescence and its protein binding properties. By complexation with serum albumin, a hydrophobic microenvironment was formed around the MNCs that activated the NIR fluorescence and provided a biomimetic surface. These results clearly confirm the potential of our method to produce stable, functional magnetic nanoclusters for multimodal theranostic applications. Further efforts will be employed to definitively tailor nanocluster size and surface functionality; moreover, we expect to extend this method to the synthesis of clinically viable hyperthermia nanoclusters, which exploit the CuAAC click reaction for the targeting of nanoclusters and real-time imaging.

METHODS

Materials. Ferrous chloride tetrahydrate ($FeCl_2$), ferric chloride hexahydrate ($FeCl_3$), ammonium hydroxide, copper(II) sulfate (Cu(II)SO_4), sodium ascorbate, azobisisobutyronitrile (AIBN), 1-nonanethiol, acrylic acid (99%), and propargyl acrylate (98%) were purchased from Sigma-Aldrich (St. Louis, MO). Inhibitor was removed from all monomers with a column of Alumina Basic (60-325 mesh). Tetrahydrofuran (THF) (HPLC grade) and dialysis tubing (SPECTRA, 10000 and 50000 MWC) were purchased from Fisher Scientific (Waltham, MA). THF was dried using a Innovative Technologies Inc. Pure Solv MD-2 solvent purification system prior to use. Deionized water was obtained from a Thermo Scientific Barnstead NANOpure system and exhibited a resistivity of $18.2 \times 10^{18}\ \Omega^{-1}\ cm^{-1}$.

Synthesis of Poly(acrylic acid) and Poly(acrylic acid-*co*-propargyl acrylate). Standard acrylic acid and clickable copolymers were synthesized by solution, free-radical polymerization. All polymerizations were performed in dry THF (2 mL) under a nitrogen atmosphere. An amount of monomer (2 g) and initiator (AIBN, 2 mg) was charged into the reaction vessel, and polymerization was allowed to proceed for 8 h. A chain transfer agent (CTA), 1-nonanethiol, was used in the polymerization reaction to tailor the molecular weight and polydispersity of the polymers. Polymers were precipitated in cold methanol, filtered, and collected. The precipitation cleaning was repeated three times in order to remove all excess monomer, initiator, and CTA.

Preparation of Magnetic Nanoclusters. Iron oxide nanoparticles were synthesized by a modified co-precipitation method. Aqueous solutions of ferric chloride ($FeCl_3$) and ferrous chloride ($FeCl_2$) were mixed in a 2:1 molar ratio in a three-necked round-bottom flask, fitted with a paddle stirring mantle, thermocouple, and nitrogen purge. $FeCl_3$ (2.703 g) and $FeCl_2$ (0.9946 g) were dissolved in deionized water (50 mL), then vigorously stirred and purged with nitrogen for 10 min. The solution was purged with nitrogen to prevent unwanted oxidation. The solution was heated to 80 °C before the dropwise addition of ammonium hydroxide (20 mL) until the solution reached pH 13. For formation of bare MMOx-NPs, stirring continued for 30 min and the solution turned from brown to black, before the reaction was stopped by exposure to air and cooling. For nanocluster formation, 0.5 g (*ca.* 13 w/w%) citric acid or polymer stabilizer was immediately added after the ammonium hydroxide, and the mixture was stirred for 90 min before cooling. The formed nanoparticles or nanoclusters were removed from solution by repeated magnetic separation and dispersion in deionized water. The final concentration of nanoparticles and nanoclusters was prepared at *ca.* 5 $mg \cdot mL^{-1}$.

Surface Modification of Magnetic Nanoclusters. Synthesis of an azido-modified ICG was reported elsewhere.[28] For a typical surface modification of the nanoclusters, azICG (5 mg), sodium ascorbate (15 mg), P(AA-PA) formed nanoclusters (10 mg), and deionized water (10 mL) were combined in a round-bottom flask. The solution was purged with nitrogen for 10 min before the addition of Cu(II)SO_4. The resulting mixture was maintained at a temperature of 28 °C for 1 h. The reaction was stopped by the removal of unreacted azICG, sodium ascorbate, and Cu(II)SO_4 through a repeated particle washing procedure consisting of magnetic collection and dispersion in water. The resulting particles were dialyzed against deionized water for 48 h at 4 °C using a dialysis bag with a 10 000 MWCO.

Characterization Methods. Molecular weights of the polymers (diluted to 1 $mg \cdot mL^{-1}$ in chloroform) were determined by gel permeation chromatography (GPC) (chloroform at 1.0 $mL \cdot min^{-1}$), using a Waters 515 pump, four 7.8 × 300 mm Styragel columns (HR 2, 3, 4, 6), a Waters 2414 refractive index detector, and a Waters 2487 tunable absorbance detector. Reported molecular weights are relative to narrow distribution polystyrene standards (M_w = 2330−980 000). High-resolution transmission electron microscopy was conducted with a Hitachi 9500. The infrared spectra were recorded at room temperature in the wavenumber range of 400−4000 cm^{-1} and referenced against air with a Nicolet 6700 FTIR spectrometer. Thermogravimetric analysis was conducted with a TA Instruments Hi-Res TGA 2950 thermogravimetric analyzer. Dried powder samples were heated at a constant rate of 20 °C · min^{-1} from 30 to 700°C under a nitrogen purge. The loss in mass after heating indicated the polymer component of nanoclusters. Hydrodynamic diameter was measured using a Coulter N4 Plus dynamic light scattering (DLS) analyzer and is reported as intensity average. Zeta-potential measurements were made with a Brookhaven Instruments Corporation ZetaPlus zeta-potential analyzer. Complex susceptibility measurements were made using an Imego DynoMag AC susceptometer. UV/vis/NIR absorbance spectra were collected using a Perkin-Elmer 900 spectrometer. Photoluminescence (PL) spectra were collected using a Thermo Oriel xenon arc lamp (Thermo Oriel 66-902) mated with a Thermo Oriel Cornerstone 7400 1/8m monochromator (Thermo Oriel 7400) and a Horiba Jobin-Yvon MicroHR spectrometer coupled to a Synapse CCD detector. All protein activation, absorbance, and fluorescence measurements were made on MNCs suspended in a PBS buffer (pH 7.4, 0.1 M).

Conflict of Interest: The authors declare no competing financial interest.

Acknowledgment. The authors thank the Gregg-Graniteville Foundation for financial support. We especially thank students in O.T. Mefford's research group at Clemson University, S. Saville and R. Stone, for their aid with magnetic measurements.

Supporting Information Available: Figures present additional TEM micrographs of the bare Fe_3O_4 nanoparticles and stabilized nanoclusters, FTIR spectra, AC susceptometry, and magnetization measurements are provided. This material is available free of charge *via* the Internet at http://pubs.acs.org.

REFERENCES AND NOTES

1. Cole, A. J.; Yang, V. C.; David, A. E. Cancer Theranostics: The Rise of Targeted Magnetic Nanoparticles. *Trends Biotechnol.* **2011**, *29*, 323–332.
2. Hao, R.; Xing, R. J.; Xu, Z. C.; Hou, Y. L.; Gao, S.; Sun, S. H. Synthesis, Functionalization, and Biomedical Applications of Multifunctional Magnetic Nanoparticles. *Adv. Mater.* **2010**, *22*, 2729–2742.
3. Miguel-Sancho, N.; Bomati-Miguel, O.; Colom, G.; Salvador, J. P.; Marco, M. P.; Santamaria, J. Development of Stable, Water-Dispersible, and Biofunctionalizable Superparamagnetic Iron Oxide Nanoparticles. *Chem. Mater.* **2011**, *23*, 2795–2802.
4. Babes, L.; Denizot, B.; Tanguy, G.; Le Jeune, J. J.; Jallet, P. Synthesis of Iron Oxide Nanoparticles Used as MRI Contrast Agents: A Parametric Study. *J. Colloid Interface Sci.* **1999**, *212*, 474–482.
5. Bin Na, H.; Palui, G.; Rosenberg, J. T.; Ji, X.; Grant, S. C.; Mattoussi, H. Multidentate Catechol-Based Polyethylene Glycol Oligomers Provide Enhanced Stability and Biocompatibility to Iron Oxide Nanoparticles. *ACS Nano* **2012**, *6*, 389–399.
6. Cho, N. H.; Cheong, T. C.; Min, J. H.; Wu, J. H.; Lee, S. J.; Kim, D.; Yang, J. S.; Kim, S.; Kim, Y. K.; Seong, S. Y. A Multifunctional Core–Shell Nanoparticle for Dendritic Cell-Based Cancer Immunotherapy. *Nat. Nanotechnol.* **2011**, *6*, 675–682.
7. Goya, G. F.; Grazu, V.; Ibarra, M. R. Magnetic Nanoparticles for Cancer Therapy. *Curr. Nanosci.* **2008**, *4*, 1–16.
8. Yu, M. K.; Jeong, Y. Y.; Park, J.; Park, S.; Kim, J. W.; Min, J. J.; Kim, K.; Jon, S. Drug-Loaded Superparamagnetic Iron Oxide Nanoparticles for Combined Cancer Imaging and Therapy *in Vivo*. *Angew. Chem., Int. Ed.* **2008**, *47*, 5362–5365.
9. Massart, R. Preparation of Aqueous Magnetic Liquids in Alkaline and Acidic Media. *IEEE Trans. Magn.* **1981**, *17*, 1247–1248.
10. Wang, Y. T.; Xu, F. H.; Zhang, C. F.; Lei, D.; Tang, Y. H.; Xu, H.; Zhang, Z. J.; Lu, H. Y.; Du, X. X.; Yang, G. Y. High MR Sensitive Fluorescent Magnetite Nanocluster for Stem Cell Tracking in Ischemic Mouse Brain. *Nanomedicine* **2011**, *7*, 1009–1019.
11. Yoon, K. Y.; Kotsmar, C.; Ingram, D. R.; Huh, C.; Bryant, S. L.; Milner, T. E.; Johnston, K. P. Stabilization of Superparamagnetic Iron Oxide Nanoclusters in Concentrated Brine with Cross-Linked Polymer Shells. *Langmuir* **2011**, *27*, 10962–10969.
12. Ge, J. P.; Hu, Y. X.; Biasini, M.; Beyermann, W. P.; Yin, Y. D. Superparamagnetic Magnetite Colloidal Nanocrystal Clusters. *Angew. Chem., Int. Ed.* **2007**, *46*, 4342–4345.
13. Ditsch, A.; Laibinis, P. E.; Wang, D. I. C.; Hatton, T. A. Controlled Clustering and Enhanced Stability of Polymer-Coated Magnetic Nanoparticles. *Langmuir* **2005**, *21*, 6006–6018.
14. Gupta, A. K.; Gupta, M. Synthesis and Surface Engineering of Iron Oxide Nanoparticles for Biomedical Applications. *Biomaterials* **2005**, *26*, 3995–4021.
15. Rutledge, R. D.; Warner, C. L.; Pittman, J. W.; Addleman, R. S.; Engelhard, M.; Chouyyok, W.; Warner, M. G. Thiol-Ene Induced Diphosphonic Acid Functionalization of Superparamagnetic Iron Oxide Nanoparticles. *Langmuir* **2010**, *26*, 12285–12292.
16. Corr, S. A.; Rakovich, Y. P.; Gun'ko, Y. K. Multifunctional Magnetic-Fluorescent Nanocomposites for Biomedical Applications. *Nanoscale Res. Lett.* **2008**, *3*, 87–104.
17. Majewski, P.; Thierry, B. Functionalized Magnetite Nanoparticles: Synthesis, Properties, and Bio-Applications. *Crit. Rev. Solid State Mater. Sci.* **2007**, *32*, 203–215.
18. Kolb, H. C.; Finn, M. G.; Sharpless, K. B. Click Chemistry: Diverse Chemical Function from a Few Good Reactions. *Angew. Chem., Int. Ed.* **2001**, *40*, 2004–2013.
19. van Dijk, M.; Rijkers, D. T. S.; Liskamp, R. M. J.; van Nostrum, C. F.; Hennink, W. E. Synthesis and Applications of Biomedical and Pharmaceutical Polymers *via* Click Chemistry Methodologies. *Bioconjugate Chem.* **2009**, *20*, 2001–2016.
20. Santra, S.; Kaittanis, C.; Grimm, J.; Perez, J. M. Drug/Dye-Loaded, Multifunctional Iron Oxide Nanoparticles for Combined Targeted Cancer Therapy and Dual Optical/Magnetic Resonance Imaging. *Small* **2009**, *5*, 1862–1868.
21. Maity, D.; Chandrasekharan, P.; Pradhan, P.; Chuang, K. H.; Xue, J. M.; Feng, S. S.; Ding, J. Novel Synthesis of Superparamagnetic Magnetite Nanoclusters for Biomedical Applications. *J. Mater. Chem.* **2011**, *21*, 14717–14724.
22. Ma, L. L.; Milner, T. E.; Johnston, K. P. Small Multifunctional Nanoclusters (Nanoroses) for Targeted Cellular Imaging and Therapy. *ACS Nano* **2009**, *3*, 2686–2696.
23. Roeder, R.; Rungta, P.; Bandera, Y. P.; Tsyalkovskyy, V.; Foulger, S. H. Colloidal Templating: Seeded Emulsion Polymerization of a Soluble Shelll with Controlled Alkyne Surface Density. *Soft Matter* **2012**, *8*, 5493–5500.
24. Lowe, A. B.; Hoyle, C. E.; Bowman, C. N. Thiol-Yne Click Chemistry: A Powerful and Versatile Methodology for Materials Synthesis. *J. Mater. Chem.* **2010**, *20*, 4745–4750.
25. van der Vorst, J. R.; Hutteman, M.; Mieog, J. S. D.; de Rooij, K. E.; Kaijzel, E. L.; Lowik, C. W. G. M.; Putter, H.; Kuppen, P. J. K.; Frangioni, J. V.; van de Velde, C. Near-Infrared Fluorescence Imaging of Liver Metastases in Rats Using Indocyanine Green. *J. Surg. Res.* **2012**, *174*, 266–271.
26. Malicka, J.; Gryczynski, I.; Geddes, C. D.; Lakowicz, J. R. Metal-Enhanced Emission from Indocyanine Green: A New Approach to *In Vivo* Imaging. *J. Biomed. Opt.* **2003**, *8*, 472–478.
27. Hao, R.; Xing, R. J.; Xu, Z. C.; Hou, Y. L.; Gao, S.; Sun, S. H. Synthesis, Functionalization, and Biomedical Applications of Multifunctional Magnetic Nanoparticles. *Adv. Mater.* **2010**, *22*, 2729–2742.
28. Rungta, P.; Bandera, Y. P.; Roeder, R. D.; Li, Y. C.; Baldwin, W. S.; Sharma, D.; Sehorn, M. G.; Luzinov, I.; Foulger, S. H. Selective Imaging and Killing of Cancer Cells with Protein-Activated Near-Infrared Fluorescing Nanoparticles. *Macromol. Biosci.* **2011**, *11*, 927–937.
29. Nel, A.; Xia, T.; Madler, L.; Li, N. Toxic Potential of Materials at the Nanolevel. *Science* **2006**, *311*, 622–627.
30. Prapainop, K.; Witter, D.; Wentworth, P. A Chemical Approach for Cell-Specific Targeting of Nanomaterials: Small-Molecule-Initiated Misfolding of Nanoparticle Corona Proteins. *J. Am. Chem. Soc.* **2012**, *134*, 4100–4103.
31. Philip, R.; Penzköfer, A.; Baumler, W.; Szeimies, R. M.; Abels, C. Absorption and Fluorescence Spectroscopic Investigation of Indocyanine Green. *J. Photochem. Photobiol., A* **1996**, *96*, 137–148.
32. Sauda, K.; Imasaka, T.; Ishibashi, N. Determination of Protein in Human-Serum by High-Performance Liquid-Chromatography with Semiconductor-Laser Fluorometric Detection. *Anal. Chem.* **1986**, *58*, 2649–2653.
33. Palma, A.; Alvarez, L. A.; Scholz, D.; Frimannsson, D. O.; Grossi, M.; Quinn, S. J.; O'Shea, D. F. Cellular Uptake Mediated Off/On Responsive Near-Infrared Fluorescent Nanoparticles. *J. Am. Chem. Soc.* **2011**, *133*, 19618–19621.
34. Weissleder, R. A Clearer Vision for *In Vivo* Imaging. *Nat. Biotechnol.* **2001**, *19*, 316–317.
35. Weissleder, R.; Tung, C.; Mahmood, U.; Bogdanov, A. *In Vivo* Imaging of Tumors with Protease-Activated Near-Infrared Fluorescent Probes. *Nat. Biotechnol.* **1999**, *17*, 375–378.
36. Lin, C. L.; Lee, C. F.; Chiu, W. Y. Preparation and Properties of Poly(acrylic acid) Oligomer Stabilized Superparamagnetic Ferrofluid. *J. Colloid Interface Sci.* **2005**, *291*, 411–420.
37. Viota, J. L.; de Vicente, J.; Duran, J. D. G.; Delgado, A. Stabilization of Magnetorheological Suspensions by Polyacrylic Acid Polymers. *J. Colloid Interface Sci.* **2005**, *284*, 527–541.
38. Mak, S. Y.; Chen, D. H. Fast Adsorption of Methylene Blue on Polyacrylic Acid-Bound Iron Oxide Magnetic Nanoparticles. *Dyes Pigm.* **2004**, *61*, 93–98.
39. Dalelio, G. F.; Evers, R. C. Linear Polymers of Some Vinyl Monomers Containing a Terminal Acetylenic Group. *J. Polym. Sci., Part A: Polym. Chem.* **1967**, *5*, 999.
40. Odian, G. G. *Principles of Polymerization*, 4th ed.; Wiley-Interscience: Hoboken, N.J., 2004.
41. Tao, K.; Song, S.; Ding, J.; Dou, H. J.; Sun, K. Carbonyl Groups Anchoring for the Water Dispersibility of Magnetite Nanoparticles. *Colloid Polym. Sci.* **2011**, *289*, 361–369.

42. Liu, J.; Sun, Z. K.; Deng, Y. H.; Zou, Y.; Li, C. Y.; Guo, X. H.; Xiong, L. Q.; Gao, Y.; Li, F. Y.; Zhao, D. Y. Highly Water-Dispersible Biocompatible Magnetite Particles with Low Cytotoxicity Stabilized by Citrate Groups. *Angew. Chem., Int. Ed.* **2009**, *48*, 5875–5879.
43. Racuciu, M.; Creanga, D. E.; Airinei, A. Citric-Acid-Coated Magnetite Nanoparticles for Biological Applications. *Eur. Phys. J. E* **2006**, *21*, 117–121.
44. Keiser, J. T.; Brown, C. W.; Heidersbach, R. H. The Oxidation of Fe_3O_4 on Iron and Steel Surfaces. *Corrosion* **1982**, *38*, 357–360.
45. Hunter, R. *Foundations of Colloid Science*, 2nd ed.; Oxford University Press: New York, 2001.
46. Xiao, L.; Li, J.; Brougham, D. F.; Fox, E. K.; Feliu, N.; Bushmelev, A.; Schmidt, A.; Mertens, N.; Kiessling, F.; Valldor, M.; Fadeel, B.; Mathur, S. Water-Soluble Superparamagnetic Magnetite Nanoparticles with Biocompatible Coating for Enhanced Magnetic Resonance Imaging. *ACS Nano* **2011**, *5*, 6315–6324.
47. Ma, M.; Wu, Y.; Zhou, H.; Sun, Y. K.; Zhang, Y.; Gu, N. Size Dependence of Specific Power Absorption of Fe_3O_4 Particles in AC Magnetic Field. *J. Magn. Magn. Mater.* **2004**, *268*, 33–39.
48. Verges, M. A.; Costo, R.; Roca, A. G.; Marco, J. F.; Goya, G. F.; Serna, C. J.; Morales, M. P. Uniform and Water Stable Magnetite Nanoparticles with Diameters Around the Monodomain-Multidomain Limit. *J. Phys. D: Appl. Phys.* **2008**, *41*, 134003.
49. Xu, F. H.; Cheng, C. M.; Xu, F. J.; Zhang, C. F.; Xu, H.; Xie, X.; Yin, D. Z.; Gu, H. C. Superparamagnetic Magnetite Nanocrystal Clusters: A Sensitive Tool for MR Cellular Imaging. *Nanotechnology* **2009**, *20*, 405102.
50. Fornara, A.; Johansson, P.; Petersson, K.; Gustafsson, S.; Qin, J.; Olsson, E.; Ilver, D.; Krozer, A.; Muhammed, M.; Johansson, C. Tailored Magnetic Nanoparticles for Direct and Sensitive Detection of Biomolecules in Biological Samples. *Nano Lett.* **2008**, *8*, 3423–3428.
51. Kim, J. S.; Ligler, F. S. Utilization of Microparticles in Next-Generation Assays for Microflow Cytometers. *Anal. Bioanal. Chem.* **2010**, *398*, 2373–2382.
52. Valenzuela, O. A.; Aquino, J. M.; Galindo, R. B.; Fernandez, O. R.; Fannin, P. C.; Giannitsis, A. T. Synthesis and Complex Magnetic Susceptibility Characterization of Magnetic Fluids in Different Liquid Carriers. *J. Appl. Phys.* **2005**, *9*, 10Q914.
53. Fannin, P. C.; Mac Oireachtaigh, C.; Cohen-Tannoudji, L.; Bertrand, E.; Bibette, J. Complex Susceptibility Measurements of a Suspension of Magnetic Beads. *J. Magn. Magn. Mater.* **2006**, *300*, E210–E212.
54. Kotitz, R.; Fannin, P. C.; Trahms, L. Time-Domain Study of Brownian and Neel Relaxation in Ferrofluids. *J. Magn. Magn. Mater.* **1995**, *149*, 42–46.
55. Fannin, P. C.; Scaife, B. K. P.; Charles, S. W. A Study of the Complex Susceptibility of Ferrofluids and Rotational Brownian-Motion. *J. Magn. Magn. Mater.* **1987**, *65*, 279–281.
56. Debye, P. J. W. *Polar Molecules*; The Chemical Catalog Company, Inc.: New York, 1929.
57. Lakhtina, E.; Pshenichnikov, A. Dispersion of Magnetic Susceptibility and the Microstructure of Magnetic Fluid. *Colloid J.* **2006**, *68*, 327–337.